IJMMM International Journal of Minerals, Metallurgy and Materials 矿物冶金与材料学报（英文版）

Prediction of the thermal conductivity of Mg–Al–La alloys by CALPHAD method

Hongxia Li, Wenjun Xu, Yufei Zhang, Shenglan Yang, Lijun Zhang, Bin Liu, Qun Luo, and Qian Li

Cite this article as:
Hongxia Li, Wenjun Xu, Yufei Zhang, Shenglan Yang, Lijun Zhang, Bin Liu, Qun Luo, and Qian Li, Prediction of the thermal conductivity of Mg–Al–La alloys by CALPHAD method, *Int. J. Miner. Metall. Mater.*, 31(2024), No. 1, pp. 129-137. https://doi.org/10.1007/s12613-023-2759-6

Articles you may be interested in

Shao-chun Chen, Hong-xiang Ye, and Xin-qiang Lin, Effect of rare earth and alloying elements on the thermal conductivity of austenitic medium manganese steel, *Int. J. Miner. Metall. Mater.*, 24(2017), No. 6, pp. 670-674. https://doi.org/10.1007/s12613-017-1449-7

Hui Xu, Jian-hao Chen, Shu-bin Ren, Xin-bo He, and Xuan-hui Qu, Sintering behavior and thermal conductivity of nickel-coated graphite flake/copper composites fabricated by spark plasma sintering, *Int. J. Miner. Metall. Mater.*, 25(2018), No. 4, pp. 459-471. https://doi.org/10.1007/s12613-018-1592-9

Amir Hossein Baghdadi, Zainuddin Sajuri, Nor Fazilah Mohamad Selamat, Mohd Zaidi Omar, Yukio Miyashita, and Amir Hossein Kokabi, Effect of intermetallic compounds on the fracture behavior of dissimilar friction stir welding joints of Mg and Al alloys, *Int. J. Miner. Metall. Mater.*, 26(2019), No. 10, pp. 1285-1298. https://doi.org/10.1007/s12613-019-1834-5

Xiang-peng Zhang, Hong-xia Wang, Li-ping Bian, Shao-xiong Zhang, Yong-peng Zhuang, Wei-li Cheng, and Wei Liang, Microstructure evolution and mechanical properties of Mg–9Al–1Si–1SiC composites processed by multi-pass equal-channel angular pressing at various temperatures, *Int. J. Miner. Metall. Mater.*, 28(2021), No. 12, pp. 1966-1975. https://doi.org/10.1007/s12613-020-2123-z

Ping-ping Wang, Guo-qin Chen, Wen-jun Li, Hui Li, Bo-yu Ju, Murid Hussain, Wen-shu Yang, and Gao-hui Wu, Microstructural evolution and thermal conductivity of diamond/Al composites during thermal cycling, *Int. J. Miner. Metall. Mater.*, 28(2021), No. 11, pp. 1821-1827. https://doi.org/10.1007/s12613-020-2114-0

Guo-zheng Kang and Hang Li, Review on cyclic plasticity of magnesium alloys: Experiments and constitutive models, *Int. J. Miner. Metall. Mater.*, 28(2021), No. 4, pp. 567-589. https://doi.org/10.1007/s12613-020-2216-8

IJMMM WeChat

QQ author group

INTERNATIONAL JOURNAL OF
Minerals, Metallurgy and Materials

Volume 31, Number 1, January 2024
Page 129

Research Article https://doi.org/10.1007/s12613-023-2759-6

Prediction of the thermal conductivity of Mg–Al–La alloys by CALPHAD method

Hongxia Li[1)], *Wenjun Xu*[1)], *Yufei Zhang*[1)], *Shenglan Yang*[2)], *Lijun Zhang*[3)], *Bin Liu*[1)], *Qun Luo*[1),✉], *and Qian Li*[1,2,4,5),✉]

1) State Key Laboratory of Advanced Special Steels & Shanghai Key Laboratory of Advanced Ferrometallurgy & School of Materials Science and Engineering, Shanghai University, Shanghai 200444, China
2) National Engineering Research Center for Magnesium Alloys, Chongqing University, Chongqing 400044, China
3) State Key Laboratory of Powder Metallurgy, Central South University, Changsha 410083, China
4) College of Materials Science and Engineering, Chongqing University, Chongqing 400044, China
5) National Key Laboratory of Advanced Casting Technologies, Chongqing University, Chongqing 400044, China
(Received: 7 August 2023; revised: 27 September 2023; accepted: 9 October 2023)

Abstract: Mg−Al alloys have excellent strength and ductility but relatively low thermal conductivity due to Al addition. The accurate prediction of thermal conductivity is a prerequisite for designing Mg−Al alloys with high thermal conductivity. Thus, databases for predicting temperature- and composition-dependent thermal conductivities must be established. In this study, Mg−Al−La alloys with different contents of Al_2La, Al_3La, and $Al_{11}La_3$ phases and solid solubility of Al in the α-Mg phase were designed. The influence of the second phase(s) and Al solid solubility on thermal conductivity was investigated. Experimental results revealed a second phase transformation from Al_2La to Al_3La and further to $Al_{11}La_3$ with the increasing Al content at a constant La amount. The degree of the negative effect of the second phase(s) on thermal diffusivity followed the sequence of Al_2La > Al_3La > $Al_{11}La_3$. Compared with the second phase, an increase in the solid solubility of Al in α-Mg remarkably reduced the thermal conductivity. On the basis of the experimental data, a database of the reciprocal thermal diffusivity of the Mg−Al−La system was established by calculation of the phase diagram (CALPHAD) method. With a standard error of ±1.2 W/(m·K), the predicted results were in good agreement with the experimental data. The established database can be used to design Mg−Al alloys with high thermal conductivity and provide valuable guidance for expanding their application prospects.

Keywords: magnesium alloy; thermal conductivity; thermodynamic calculations; materials computation

1. Introduction

Among magnesium alloys, Mg–Al alloys have excellent strength and ductility and the advantages of light weight, good corrosion resistance, and easy processing, making them an ideal structural material [1–7]. However, Al addition to the α-Mg matrix significantly reduces the thermal conductivity of Mg alloys [8–10] because the solute atoms and the second phase hinder phonon and electron scattering, inevitably reducing the thermal conductivity [11–14]. Therefore, improving the thermal conductivity of Mg–Al alloys has become a key goal of current studies [15–16]. The solid solution of alloying elements causes lattice distortion and disrupts the lattice periodicity, resulting in a significant reduction in thermal conductivity compared with the formation of the second phase [5,17–20]. Adding rare earth elements, such as lanthanum (La), cerium (Ce), gadolinium (Gd), and yttrium (Y), could improve the thermal conductivity to achieve the desirable comprehensive performance of Mg alloys [21–25]. La and Ce are more economical than other heavy rare earth elements, and their solid solubilities in Mg alloys are lower [26]. Compared with Ce, La has a lower effect on reducing thermal conductivity [17]. Therefore, La is the optimal alloying element.

Mg–Al–La alloys have attracted attention due to their excellent mechanical properties, high-temperature thermal stability, and good thermal conductivity [26–29]. The La in the alloy combines with the Al to form the $Al_{11}RE_3$ phase, which has a high melting point and thermal stability [30–32] and can significantly reduce the Al content in the α-Mg matrix and improve the thermal conductivities of the alloy [33]. In addition, the solid solubility of La in the α-Mg matrix is very low, and Mg–Al–La alloys show good thermal conductivity [34–35]. Mg–Al–La alloys have many second phases, such as $LaMg_{12}$, Al_2La, Al_3La, and $Al_{11}La_3$, which have different effects on thermal conductivity [36–37]. However, current research on the thermal conductivity of Mg–Al–La alloys mainly focuses on changing the content of La or Al to obtain alloys with mechanical properties and thermal conductivity. The effects of solute atoms and the second phase on thermal

✉ Corresponding authors: Qun Luo E-mail: qunluo@shu.edu.cn; Qian Li E-mail: cquliqian@cqu.edu.cn

conductivity have not been studied in depth, thus limiting the selection and design range of alloy components.

With the use of calculation of the phase diagram (CALPHAD) to determine the thermal conductivity of the alloys, extensive experiments to obtain the composition range of the alloy can be avoided [38–40]. The relationship between thermal conductivity and phases can be established by combining CALPHAD with less experimental data to predict the thermal conductivity of a wide range of alloy compositions and explore the influence of different second phases on thermal conductivity [41–43]. CALPHAD has been successfully applied in the calculation of the thermal conductivity of Mg and Al alloys [44–45]. Wang *et al*. [46] utilized this method to investigate the influence of alloying elements and second phases on the thermal conductivity of Al alloys. Huang *et al*. [44] and Zhang *et al*. [47] established thermal conductivity models within the CALPHAD framework to calculate the thermal conductivity of Mg–Al–Zn and Al–Cu–Mg–Si systems, respectively. Our previous work [17] proposed a method for predicting thermal conductivity based on reciprocal thermal diffusivity (RTD), also known as thermal diffusion resistivity. This method accurately predicts the thermal conductivity of Mg–Zn–La/Ce systems by establishing a relationship between the thermal diffusion resistivity and temperature. The predicted accuracy of the thermal conductivity was within 1.6%.

In this work, CALPHAD was used to establish the relationship between the RTD and temperature in the Mg–Al–La system, covering the thermal conductivity of elements, solid solutions, intermetallic compounds, and interaction among phases. The influence of different second phases and Al solid solubility on the microstructure and thermal conductivity of Mg–Al–La alloys were also studied. Moreover, the thermal conductivities of Mg–Al–La alloys were predicted using the obtained database of thermal diffusion resistivity.

2. Experimental

From the thermodynamic database of the Mg–Al–La alloy system [48], the correlation between the key intermetallics $LaMg_{12}$, Al_2La, Al_3La, and $Al_{11}La_3$ and the α-Mg matrix phase was determined as shown in Fig. 1(a). The experimental samples were designed and distributed within the Mg-rich composition range of Mg–Al–La alloys (0–4at% Al and 0–1at% La) in accordance with the three alloy design principles as follows [17]: (1) containing different types of intermetallic compounds, such as Al_2La, Al_3La, or $Al_{11}La_3$; (2) containing the same intermetallic compound but with different contents in the range of 0.5mol%–3mol%; (3) having different Al solubilities in the α-Mg matrix. Several experimental points (#L1–#L6) in the two-phase regions of α-Mg+Al_2La, α-Mg+Al_3La, and α-Mg+$Al_{11}La_3$ were selected, and the content of the second phase was 0.6mol% and 1.8mol%.

The raw materials were Mg with a purity of 99.99%, Al with a purity of 99.99%, and La with a purity of 99.99%. As-cast Mg–Al–La alloys were prepared using an SG2-5-10 vertical resistance furnace under the protection of a mixed gas of SF_6+CO_2 (the volume ratio is 1:40) and then cooled in a steel mold by gravity casting to obtain a cylindrical ingot with a weight of 100 g. Afterward, 2wt% of Mg and 5wt% of Al were added to offset the weight loss, control the loss of alloying elements, and achieve compositions close to the designed alloys. In brief, 30 g of three different Al–La intermetallic compounds, Al_2La, Al_3La, and $Al_{11}La_3$, were prepared using a WK-II non-consumable vacuum arc melting furnace under the protection of pure Ar. Each sample was remelted five times during melting to ensure the homogeneity of the alloy composition. The actual compositions of the designed alloys were examined using inductively coupled plasma atomic emission spectrometry (ICP). The microstructure of the alloy was observed by scanning electron microscopy backscattering mode (SEM–BSE) combined with energy dispersive spectroscopy (EDS) to determine the composition of the phases. The thermal diffusivity of the alloys was measured using a Netzsch LFA467 device. The samples used for thermal conductivity testing were cut in a disc shape with dimensions of ϕ10 mm × 3 mm from 10 mm above the bottom of the ingots and then subjected to laser flash analysis

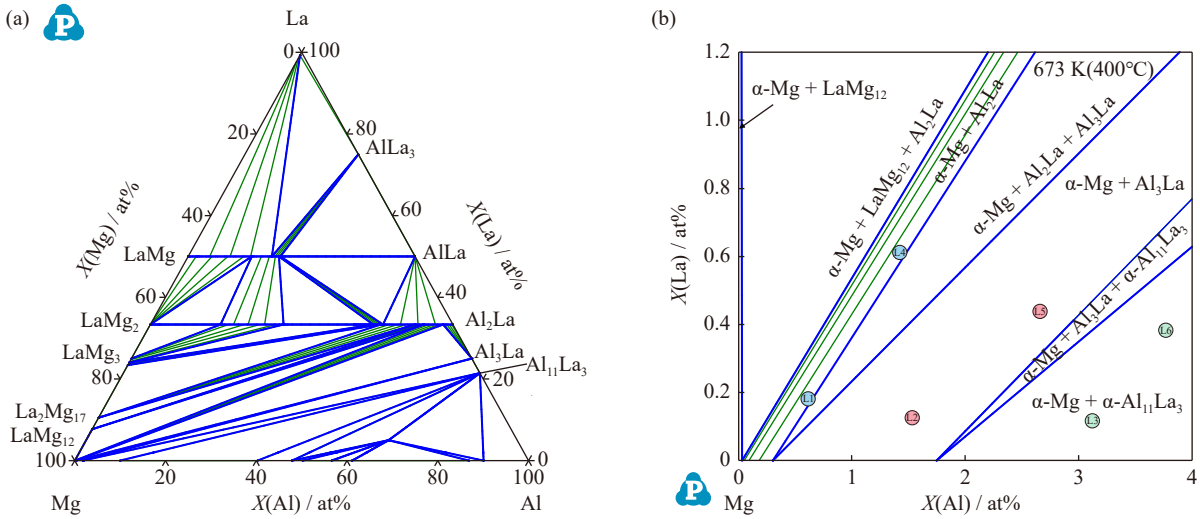

Fig. 1. Isothermal section of the Mg–Al–La system at 673 K: (a) full composition range; (b) Mg-rich corner containing the constituent points of the designed alloys.

in the temperature range of 323–523 K.

3. CALPHAD modeling of thermal conductivity

The thermal conductivity of the alloy was calculated as the product of density, thermal diffusivity, and specific heat capacity [17], and the calculation formula is as follows:

$$\lambda = \alpha \cdot \rho \cdot C_p \quad (1)$$

where α is the thermal diffusivity (mm^2/s), ρ is the density (g/cm^3), and C_p is the specific heat capacity ($J \cdot g^{-1} \cdot K^{-1}$). The density and specific heat capacity of the alloy at different temperatures can be calculated either using the PANDAT software [45] and the thermodynamic database of the Mg–Al–La system or the experimental data. For instance, the room temperature density can be measured by the Archimedes drainage method, and the relationship between the density and temperature of the alloy at high temperatures can be obtained according to the following formula [5]:

$$\rho_{(T)} = \rho_0 - 0.156 \cdot (T - 298.15) \quad (2)$$

where $\rho_{(T)}$ is the density of the alloy at T temperature, ρ_0 (g/cm^3) is the density of the sample at 298.15 K, and T (K) is the temperature.

The specific heat capacity can be directly measured by Netzsch 204HP or calculated according to the Neumann–Kopp rule [49] for alloys with few alloy elements; that is, the specific heat of the alloy is equal to the sum of the specific heat of each element:

$$C_p = \Sigma(C_{pi} W_i) \quad (3)$$

where C_{pi} is the specific heat of each alloy element i, and W_i is the mass percentage of the alloy element i in the alloy.

For calculation, thermal conductivity was defined as RTD, also known as thermal diffusion resistance. It can be used to describe the thermal diffusivity of single-phase, solid solution, and multiphase alloys. Furthermore, thermal diffusivity can be experimentally obtained, and the use of RTD can reduce the accumulation of errors in the product of density and specific heat capacity during calculation with Eq. (1) [17].

The RTD of pure element i (RTD_i) is as follows:

$$RTD_i = a + b \cdot T + \frac{C}{T} \quad (4)$$

where a, b, and c are parameters to be optimized.

The RTD of solid solution and intermetallic compound is as follows:

$$RTD^{\varphi} = \Sigma x_i RTD_i + \Sigma x_i x_j \Sigma L_{ij}^k (x_i - x_j)^k \quad (5)$$

where x_i and x_j are the mole fraction of element i and j, respectively, L_{ij}^k is the k-th order interaction parameter between alloy elements i and j, and RTD^{φ} is the thermal diffusion resistivity of phase φ. The RTD of multiphase alloy (RTD^{alloy}) is as follows:

$$RTD^{alloy} = \Sigma f_{\varphi} RTD^{\varphi} + \Sigma f_{\varphi} f_{\tau} \Sigma M_{\varphi\tau}^k (f_{\varphi} - f_{\tau})^k \quad (6)$$

where f_{φ} and f_{τ} are the mole fraction of phases φ and τ, respectively. $M_{\varphi\tau}^k$ is the k-th order interaction parameter of phases φ and τ.

The thermal diffusivity of any alloy can be calculated as

$$\alpha = 1/RTD^{alloy} \quad (7)$$

The thermal conductivity of alloys is predicted as

$$\lambda = \frac{1}{RTD^{alloy}} \cdot \rho \cdot C_p \quad (8)$$

All the interaction parameters must be optimized by assessing the experimental thermal diffusivity data.

The standard error (SE) between experimentally measured and model-predicted thermal conductivities (σ_{SE}) is given as [50]

$$\sigma_{SE} = \sqrt{\frac{\sum_{i=1}^{n} (\lambda_{Exp} - \lambda_{Cal})^2}{(n-1)}} \quad (9)$$

where λ_{Exp} represents the experimental value, λ_{Cal} represents the calculated value, and n represents the number of samples. The smaller the SE, the higher the consistency between the experimental and calculated values.

4. Results and discussion

4.1. Phases and microstructures of as-cast Mg–Al–La alloys

All the designed Mg–Al–La alloys are in the two-phase region of the Mg-rich corner and contain a small amount of the second phase, as shown in Fig. 1. The alloys with the same second phase are marked with the same shape and color. Given the similarity of the alloy system, the solidification of alloys with different phases was evaluated using the Lever rule [17,43]. The corresponding alloy phase constitution and Al solubility in the α-Mg phase were obtained as listed in Table 1. The actual compositions of the experimental alloys determined by ICP are also shown in Table 1. A comparison of phase contents among different Mg alloys reveals that the intermetallic compound phase fraction of the #L4–#L6 alloys is 1.2mol% higher than that of the #L1–#L3 alloys. Therefore, the #L4–#L6 alloys have a higher content of intermetallic compound phases compared with the alloys designed in the same group. As a consequence, morphological observation

Table 1. Actual compositions, phases, and Al solid solubility in the α-Mg matrix of the designed alloys

Alloy in Mg–Al–La system	Phase contents	Solubility of Al in α-Mg / at%
#L1 ($Mg_{99.15}Al_{0.66}La_{0.19}$)	α-Mg + 0.6mol% Al_2La	0.29
#L2 ($Mg_{98.30}Al_{1.46}La_{0.14}$)	α-Mg + 0.6mol% Al_3La	1.05
#L3 ($Mg_{96.91}Al_{2.96}La_{0.13}$)	α-Mg + 0.6mol% $Al_{11}La_3$	2.50
#L4 ($Mg_{97.94}Al_{1.46}La_{0.60}$)	α-Mg + 1.8mol% Al_2La	0.31
#L5 ($Mg_{96.92}Al_{2.64}La_{0.44}$)	α-Mg + 1.8mol% Al_3La	1.35
#L6 ($Mg_{95.92}Al_{3.69}La_{0.39}$)	α-Mg + 1.8mol% $Al_{11}La_3$	2.30

and phase analysis of these alloys can be easily performed.

Fig. 2(a)–(c) shows the backscattered SEM images of as-cast #L4–#L6 Mg alloys. Fig. 2(d)–(i) displays the EDS energy spectrum analysis at the corresponding points selected in point scan mode in Fig. 2(a)–(c), and Table 2 gives the element content of different phase compositions at point d–i. A large amount of the second phase is distributed along the interdendritic boundaries. With the increasing Al content, the types and micromorphology of the second phase in the alloys change noticeably. In terms of micromorphology, the second phase near the grain boundaries changes from a continuous network structure (Al_2La and Al_3La) to a discontinuous lamella-like structure ($Al_{11}La_3$). As shown in the backscattered SEM images of Fig. 2(a), the second phase in the $Mg_{97.94}Al_{1.46}La_{0.60}$ alloy is distributed at the grain boundary in the form of a network structure. EDS analysis of d and e points in Fig. 2(a) reveals that the gray area has a Mg content exceeding 99.0at% and thus was identified as the α-Mg phase. The atomic ratio of Al and La in the network's second phase is 2.1:1, which is consistent with that in the Al_2La phase. With the increase in Al content, the distribution of the second phase in the $Mg_{96.92}Al_{2.64}La_{0.44}$ alloy (Fig. 2(b)) increases compared with that in the $Mg_{97.94}Al_{1.46}La_{0.60}$ alloy (Fig. 2(a)). This phenomenon may be due to the increase in Al content and the preferential combination of Al and La to form many intermetallic compounds, causing an increase in the content of the second phase. EDS analysis of point g in Fig. 2(b) reveals that the atomic ratio of Al and La in the network's second phase is 3.1:1, which is consistent with that in the Al_3La phase. In the $Mg_{95.92}Al_{3.69}La_{0.39}$ alloy (Fig. 2(c)), the second phase transforms from a continuous network to a discontinuous network and presents a lamella-like distribution along the grain boundaries. EDS analysis of point i in Fig. 2(c) shows that the atomic ratio of Al and La in the lamella-like second phase is 11.1:3, which is close to that in the $Al_{11}La_3$ phase.

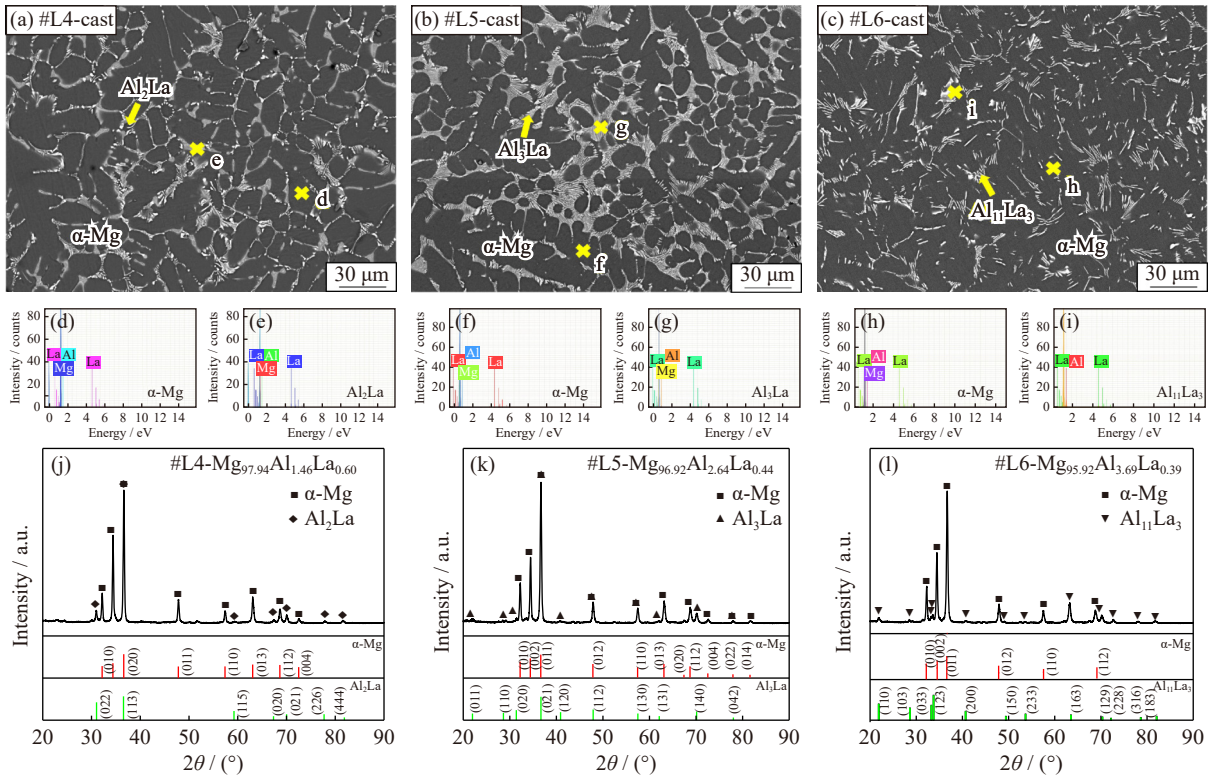

Fig. 2. (a–c) BSE images of as-cast #L4-#L6 Mg–Al–La alloys; (d–i) phase content of EDS energy spectrum analysis corresponding to the points in (a–c); (j–l) XRD patterns of #L4–#L6 alloys.

During the quantitative analysis of phase content using EDS, data errors are inevitably introduced due to the detection of α-Mg content. Therefore, the second phase composition was further determined using X-ray diffraction (XRD). Fig. 2(j)–(l) shows the XRD patterns of the #L4–#L6 alloys. Measurement of phase composition reveals that the #L4–#L6 alloys contain different intermetallic compounds, which is consistent with the design and EDS results.

4.2. Effect of intermetallic compounds and solid solubility on the thermal diffusivity of Mg–Al–La alloys

The thermal diffusivities of Mg–Al–La alloys are affected by the α-Mg phase and the surrounding second phases [19]. Fig. 3 shows the experimentally measured thermal diffusivities of the designed Mg–Al–La alloys. In Fig. 3(a)–(c), the same shape symbols represent Mg–Al–La dual-phase alloys with different types but the same second-phase content. For the Mg–Al–La alloys with the same kind of second phase, their thermal diffusivities show a tendency to decrease with the increase in the second phase content from 0.6mol% to 1.8mol% (Fig. 3(a)–(c)). This change may be attributed to the introduction of additional phase and grain boundaries into the alloy as the content of the second phase increases; as a consequence, the lattice distortion intensifies, which in turn

Table 2. EDS analysis showing the different element contents at points d–i of #L4–#L6 alloys in Fig. 2(a)–(c)

Alloy type	Sampling point	Element content / at%		
		Mg	Al	La
#L4 alloy	d	99.38	0.48	0.03
	e	98.98	0.89	0.43
#L5 alloy	f	99.18	0.78	0.04
	g	94.04	4.49	1.47
#L6 alloy	h	98.49	1.49	0.02
	i	84.69	12.08	3.26

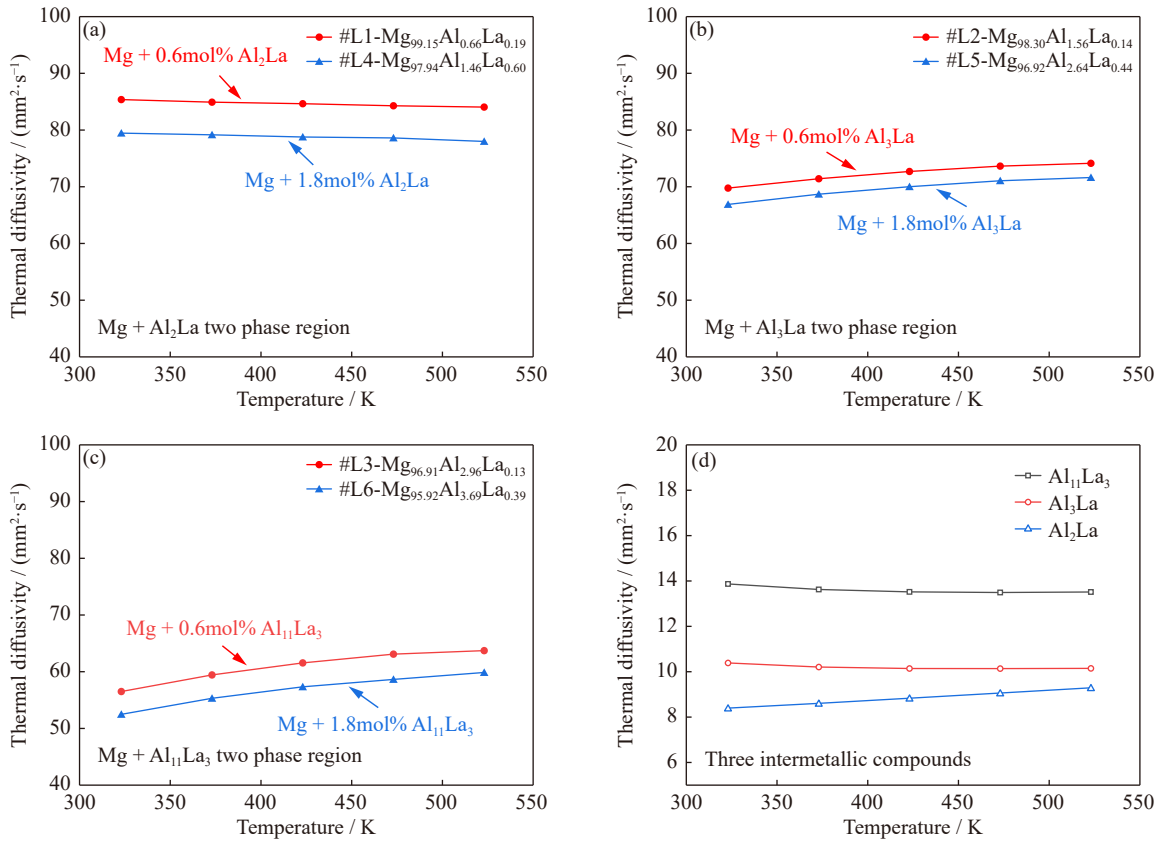

Fig. 3. Experimentally measured thermal diffusivities of (a–c) as-cast #L1-#L6 alloys and (d) three intermetallic compounds.

hinders the free movement of electrons and phonons and thereby reduces the thermal diffusivity [8,17].

The experimental thermal diffusivities of Mg–Al–La alloys with the same phase content (i.e., 0.6mol% or 1.8mol%) but different types of second phases follow the sequence of α(α-Mg+Al_2La) > α(α-Mg+Al_3La) > α(α-Mg+$Al_{11}La_3$). In particular, the thermal diffusivities of the alloys containing the Al_2La phase are 18.1–26.9 mm^2/s higher than those of the alloys containing the $Al_{11}La_3$ phase. Meanwhile, the thermal diffusivities of the alloys containing the Al_3La phase are 11.8–14.8 mm^2/s higher than those of the alloys containing the $Al_{11}La_3$ phase. This finding indicates that different types of second phases have distinct effects on the thermal conductivity of the alloy. For example, Zhao *et al.* [26] showed that when the Al content (X) increased in the Mg–4La–XAl–0.5Mn alloy, the second phase changed from a single $LaMg_{12}$ to a small amount of Al_2La grown in $LaMg_{12}$ and the thermal conductivity showed a slight upward trend. Xie *et al.* [17] pointed out that when the content of the second phase $LaMg_{12}$ in the Mg–Zn–La alloy increased from 4.7mol% to 7.3mol%, the thermal conductivity of the alloy decreased by 8–11 W/(m·K), indicating that an increase in phase content results in a decrease in thermal conductivity. Su *et al.* [51] observed that as the Ce content increased in the Mg–Ce alloy, the second phase transformed from the discontinuous distribution of $Mg_{12}Ce$ in the Mg–0.4Ce alloy into the continuous network of $Mg_{17}Ce_2$ in the Mg–1.5Ce alloy.

Three Al–La single-phase alloys (Al_2La, Al_3La, and $Al_{11}La_3$) were directly prepared, and their thermal conductivities were experimentally investigated to further clarify how much the different intermetallic compounds in the Mg–Al–La alloys contribute to the thermal conductivity. As shown in Fig. 3(d), the thermal diffusivities of the Al–La single-phase alloys are smaller than those of the α-Mg matrix (up to 69.3 mm^2/s, which is according to 156 W/(m·K)) [52], and the thermal diffusivities were in the sequence of $\alpha(Al_{11}La_3) > \alpha(Al_3La) > \alpha(Al_2La)$. Among the three different intermetallic compounds, Al_2La will have the largest negat-

ive impact on the thermal diffusivity of Mg alloys, and $Al_{11}La_3$ has the least negative impact. However, the results of thermal diffusivities of the two-phase alloys (α-Mg + intermetallic compound) are contrary to those observed in single-phase alloys that the ternary alloy located in the α-Mg+$Al_{11}La_3$ two-phase region exhibits the lowest thermal diffusivity, although the $Al_{11}La_3$ phase has the smallest negative impact on the thermal diffusivity in single-phase alloys. It suggests that some factors have more important effect on thermal diffusivity.

To explain this phenomenon, the effect of the solid solubility of elements in the α-Mg matrix phase on the thermal diffusivity of the alloy must be considered. Su *et al*. [51] and Xie *et al*. [17] showed that the increase in thermal resistance induced by the solid solution of alloying elements in the α-Mg matrix was approximately one order of magnitude higher than that caused by the second phase. Numerous studies also showed that the solid solubility of elements in the matrix had the most critical impact on the thermal diffusivity of the alloy compared with the type and content of the second phase [15,17,19,26,51]. The higher the solid solubility, the lower the thermal diffusivity of the alloy. In the present study, Table 1 summarizes the solid solubility of Al atoms in the α-Mg matrix in different ternary alloys. In the α-Mg+$Al_{11}La_3$ two-phase region of the alloy, the maximum solubility of Al in α-Mg is as high as 2.50at%. By contrast, the alloys containing the Al_2La phase have a low solid solubility of 0.29at%–0.31at%. This finding indicates that even if the alloy contains the $Al_{11}La_3$ phase, which has the smallest impact on thermal conductivity, the thermal conductivity of the alloy in the α-Mg+$Al_{11}La_3$ two-phase region is still greatly reduced. The main reason is the increase in the Al solid solubility in α-Mg, which significantly reduces the thermal conductivity compared with the second phase.

4.3. Prediction of thermal diffusion coefficient and thermal conductivity of the Mg–Al–La system

The thermal conductivity of Mg–Zn–La/Ce alloys was successfully predicted by constructing an expression of the RTD, which shows the relationship between thermal diffusion resistance and temperature [17]. Moreover, the experimental thermal diffusivity values were selected for parameter conversion, which can avoid calculation errors caused by the different sources of density and specific heat capacity during the calculation of thermal conductivity. Therefore, the same expression was used to describe the thermal diffusion resistance of elements, intermetallic compounds, solid solutions, and multiphase alloys for the Mg–Al–La alloy system. Finally, the thermal conductivity of the Mg–Al–La alloy was calculated.

The parameters to be optimized and the interaction parameters are based on the experimental data and are evaluated by the Pan Optimizer of PANDAT using CALPHAD. In establishing the thermal conductivity databases of Mg–Al–La alloys, some other thermodynamic parameters must be considered, including density, specific heat capacity, elemental solid solubility, and the second phase fraction, which can be calculated using the phase diagram thermodynamic database [48]. Given that the solid solubility of La in the α-Mg phase is very low, Mg and Al play a major role in the thermal conductivity of the Mg–Al–La system. The experimental data for pure Al and that in the α-Mg+$Mg_{17}Al_{12}$ two-phase region were adopted from the works of Ho [52] and Huang [44], respectively. The expression of pure metal Mg and intermetallic compound $LaMg_{12}$ in the Mg–Al–La alloy was obtained from literature [17], as shown in Table 3.

Table 3. Optimized parameters (*a*, *b*, and *c*) between temperature and the thermal diffusion resistivity of pure elements and intermetallic compounds

Element/Phase	RTD evaluated equation	Reference
Mg	$10.614 + 0.004T - 103.692T^{-1}$	[17]
Al	$3.454 + 0.012T + 953.16T^{-1}$	[47]
$LaMg_{12}$	$35.186 - 0.003T + 8018.229T^{-1}$	[17]
$Mg_{17}Al_{12}$	$-158.618 + 0.207T + 57581.880T^{-1}$	[41]
Al_2La	$133.26 - 0.052T + 888.09T^{-1}$	This work
Al_3La	$135.75 - 0.040T - 8577.556T^{-1}$	This work
$Al_{11}La_3$	$102.343 - 0.030T - 6637.071T^{-1}$	This work

The same test method and equipment were used to obtain the thermal diffusivity of binary Al–La single-phase alloys and ternary design alloys to avoid errors caused by different experimental tests. On the basis of the experimental data, thermodynamic calculations were performed by the Pan Optimizer of PANDAT, and the optimized parameters for calculating the thermal diffusion resistance of pure elements and intermetallic compound phases are listed in Table 3. Table 4

Table 4. Calculation parameters for the thermal diffusion resistivity of Mg–Al–La alloys in the solid solution and two-phase regions

Alloy system	Phase region	Assessed parameter
Mg–Al	α-Mg	$L^0_{(Mg,Al)} = 222.4 - 6.728T$
		$L^1_{(Mg,Al)} = 202.2 + 6.947T$
	α-Mg+$Mg_{17}Al_{12}$	$M^0_{HCP+Mg_{17}Al_{12}} = -158.4 + 0.316T$
		$M^1_{HCP+Mg_{17}Al_{12}} = 257.9 - 0.584T$
Mg–La	α-Mg+$LaMg_{12}$	$M^0_{HCP+LaMg_{12}} = 19.0 + 0.168T$
		$M^1_{HCP+LaMg_{12}} = -63.5 - 0.166T$
Mg–Al–La	α-Mg+Al_2La	$M^0_{HCP+Al_2La} = 1306.0 + 18.357T$
		$M^1_{HCP+Al_2La} = -1313.0 - 19.248T$
	α-Mg+Al_3La	$M^0_{HCP+Al_3La} = -3771.5 + 43.330T$
		$M^1_{HCP+Al_3La} = 3876.0 - 45.496T$
	α-Mg+$Al_{11}La_3$	$M^0_{HCP+Al_{11}La_3} = -69.8 + 199.944T$
		$M^1_{HCP+Al_{11}La_3} = 46.1 - 48.582T$

Note: HCP—hexagonal close packed.

shows the optimized parameters for thermal diffusion resistance in the solid solution and two-phase regions.

Fig. 4 shows the calculated curves of the thermal conductivities of alloys located in different two-phase regions using the established Mg–Al–La alloy thermal conductivity database. The calculated thermal conductivities are in good agreement with the experimental data, showing that the thermal conductivity of the alloy decreases gradually with the increase in alloy elements and second-phase content. In particular, the Al solid solubility in α-Mg has a greater influence on the reduction of thermal conductivity compared with the second phase.

Fig. 5(a) shows the predicted thermal conductivity distribution of the Mg–Al–La system at 323 K. The thermal conductivity of the ternary alloy shows a decreasing trend with the increase in Al and La contents. Different second phases have different effects on thermal conductivity. As the second phase transforms from Al_2La to Al_3La and then to $Al_{11}La_3$, the thermal conductivity of the alloy shows a downward trend. In the range of X(Al) > 0.5at%, the thermal conductivity region in the α-Mg+Al_2La two-phase region is higher than that in the surrounding three-phase region.

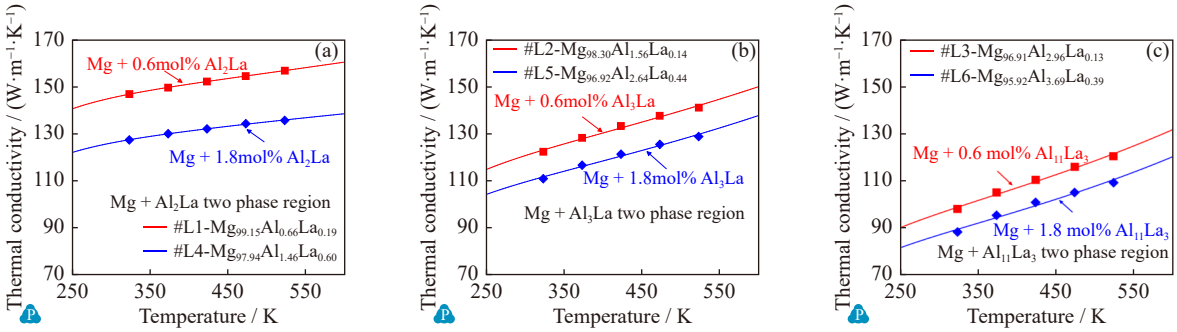

Fig. 4. Calculated thermal conductivity of as-cast #L1–#L6 alloys.

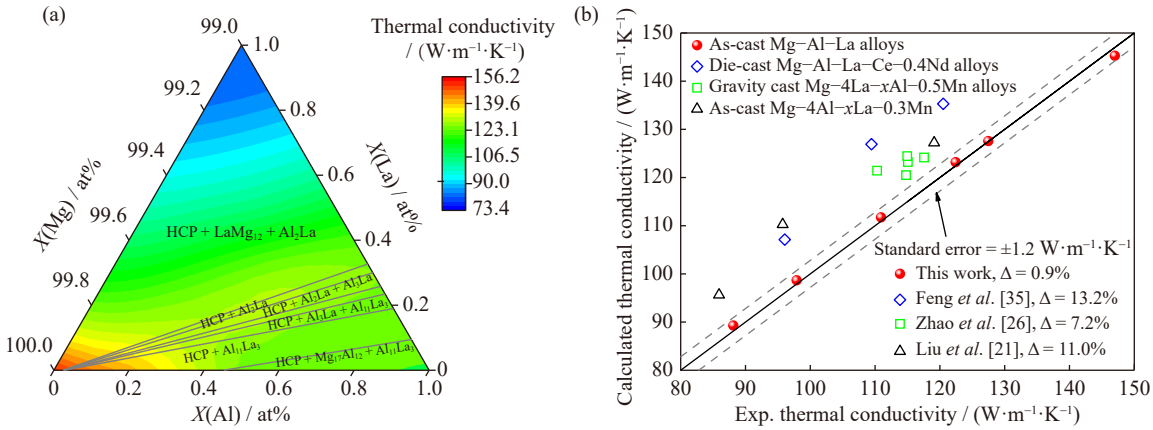

Fig. 5. (a) Predicted thermal conductivity of the Mg–Al–La system at 323 K; (b) comparison between calculated and experimentally measured thermal conductivities.

Fig. 5(b) shows the comparison between the experimental and calculated thermal conductivities of the Mg–Al–La alloy at 323 K. The calculated results show a SE of ±1.2 W/(m·K) and a relative deviation of 0.9% with self-tested experimental values. Compared with other experimental data, the relative deviation of the prediction (Δ) ranges from 7.2% to 13.2%. Analysis revealed the following sources of error: (1) different alloy compositions affect the solid solubility of solute atoms and intermetallic compounds in the α-Mg, thereby affecting the thermal conductivity of the alloy. For example, Feng *et al.* [34] added 0.4wt% Nd and 0.2wt% Mn on Mg2.8–3.7Al3.3–4.4La alloy, introduced new elements and formed the $Al_{10}RE_2Mn_7$ phase, and replaced La with Ce to obtain the thermal conductivity of the AE44 alloy. For the same Mg–Zn system, the reduction in thermal conductivity caused by Ce addition was greater than that caused by La addition at the same content, proving that the addition of different elements at the same amounts affects the thermal conductivity [17]. (2) Different experimental test conditions and operations will lead to different thermal diffusivities. Different preparations have varying cooling rates, resulting in different solid solubilities and intermetallics in alloys. (3) Effect of precipitates during heating: the precipitates formed during heating may affect the deviation of thermal diffusivity from that of the original alloy [17,53].

5. Conclusions

In this study, the influence of the second phase and solid solubility on the thermal conductivity of Mg–Al–La alloys was explored by measuring the thermal diffusivity of $Mg_{95.92–98.3}Al_{1.46–3.69}La_{0.13–0.60}$ alloys. A set of evaluation para-

meters for the thermal diffusion resistance of the Mg–Al–La alloy system in the CALPHAD type database was obtained by optimizing the experimental data. With these parameters, the thermal conductivities of alloys with different compositions and at different temperatures can be quantitatively predicted. The conclusions are summarized as follows.

(1) Different types and contents of intermetallic compounds have different effects on the thermal conductivity. The degree of the negative influence of different intermetallic compounds on the thermal diffusivity follows the sequence of Al_2La > Al_3La > $Al_{11}La_3$. With the increase in its second-phase content, the thermal conductivity of the alloy decreases gradually.

(2) Compared with the second phase, the Al solid solubility in the α-Mg phase significantly affects the thermal conductivity. When the Al solid solubility is high, the thermal conductivity decreases significantly.

(3) The evaluation parameters of the thermal diffusion resistance of the alloy system are obtained from the experimental data by establishing the relationship between the thermal diffusion resistance and temperature. The calculated SE of the self-test value reaches ±1.2 W/(m·K).

Acknowledgements

This work was financially supported by the National Key Research and Development Program of China (No. 2021YFB3701001), the National Natural Science Foundation of China (No. U2102212), the Shanghai Rising-Star Program (No. 21QA1403200), and the Shanghai Engineering Research Center for Metal Parts Green Remanufacture (No. 19DZ2252900) from Shanghai Engineering Research Center Construction Project.

Conflict of Interest

Qian Li and Qun Luo are an editorial board member and a youth editorial board member for IJMMM, respectively, and are not involved in the editorial review or the decision to publish this article. All authors declare that they have no financial interests or personal relationships that could have appeared to influence the work reported in this paper.

References

[1] B. Liu, J. Yang, X.Y. Zhang, Q. Yang, J.S. Zhang, and X.Q. Li, Development and application of magnesium alloy parts for automotive OEMs: A review, *J. Magnes. Alloys*, 11(2023), No. 1, p. 15.

[2] J.F. Song, J. She, D.L. Chen, and F.S. Pan, Latest research advances on magnesium and magnesium alloys worldwide, *J. Magnes. Alloys*, 8(2020), No. 1, p. 1.

[3] P.P. Wang, H.T. Jiang, Y.J. Wang, *et al*., Role of trace additions of Ca and Sn in improving the corrosion resistance of Mg–3Al–1Zn alloy, *Int. J. Miner. Metall. Mater.*, 29(2022), No. 8, p. 1559.

[4] K. Yang, H.C. Pan, S. Du, *et al*., Low-cost and high-strength Mg–Al–Ca–Zn–Mn wrought alloy with balanced ductility, *Int. J. Miner. Metall. Mater.*, 29(2022), No. 7, p. 1396.

[5] S.B. Li, X.Y. Yang, J.T. Hou, and W.B. Du, A review on thermal conductivity of magnesium and its alloys, *J. Magnes. Alloys*, 8(2020), No. 1, p. 78.

[6] Q. Luo, Y.L. Guo, B. Liu, *et al*., Thermodynamics and kinetics of phase transformation in rare earth–magnesium alloys: A critical review, *J. Mater. Sci. Technol.*, 44(2020), p. 171.

[7] H.B. Liao, L.L. Mo, X. Zhou, Z.Z. Yuan, and J. Du, Revealing the nucleation event of Mg–Al alloy induced by Fe impurity, *Int. J. Miner. Metall. Mater.*, 29(2022), No. 7, p. 1317.

[8] J. Rong, W.L. Xiao, X.Q. Zhao, *et al*., High thermal conductivity and high strength magnesium alloy for high pressure die casting ultrathin-walled components, *Int. J. Miner. Metall. Mater.*, 29(2022), No. 1, p. 88.

[9] H.C. Chen, T.C. Xie, Q. Liu, *et al*., Mechanism and prediction of aging time related thermal conductivity evolution of Mg–Zn alloys, *J. Alloys Compd.*, 930(2023), art. No. 167392.

[10] V.E. Bazhenov, A.V. Koltygin, M.C. Sung, *et al*., Development of Mg–Zn–Y–Zr casting magnesium alloy with high thermal conductivity, *J. Magnes. Alloys*, 9(2021), No. 5, p. 1567.

[11] H.G. Zhong, Z.H. Lin, Q.Y. Han, *et al*., Hot tearing behavior of AZ91D magnesium alloy, *J. Magnes. Alloys*, (2023) DOI: 10.1016/j.jma. 2023.02.010

[12] G.Y. Yuan, G.Q. You, S.L. Bai, and W. Guo, Effects of heat treatment on the thermal properties of AZ91D magnesium alloys in different casting processes, *J. Alloys Compd.*, 766(2018), p. 410.

[13] Y.X. Zhang, H.H. Kang, H. Nagaumi, and X.Y. Yang, Tracing the microstructures, mechanical properties and thermal conductivity of low-temperature extruded MgMn alloys with various cerium additions, *Mater. Charact.*, 196(2023), art. No. 112658.

[14] H.B. Ma, J.H. Wang, H.Y. Wang, *et al*., Influence of nano-diamond content on the microstructure, mechanical and thermal properties of the ZK60 composites, *J. Magnes. Alloys*, 10(2022), No. 2, p. 440.

[15] L.P. Zhong, J. Peng, S. Sun, Y.J. Wang, Y. Lu, and F.S. Pan, Microstructure and thermal conductivity of As-cast and As-solutionized Mg–rare earth binary alloys, *J. Mater. Sci. Technol.*, 33(2017), No. 11, p. 1240.

[16] F.J. Yao, G.Q. You, S. Zeng, D.S. Lu, and Y. Ming, Reaction-tunable diffusion bonding to multilayered Cu mesh/ZK61 Mg foil composites with thermal conductivity and lightweight synergy, *J. Mater. Sci. Technol.*, 139(2023), p. 10.

[17] T.C. Xie, H. Shi, H.B. Wang, Q. Luo, Q. Li, and K.C. Chou, Thermodynamic prediction of thermal diffusivity and thermal conductivity in Mg–Zn–La/Ce system, *J. Mater. Sci. Technol.*, 97(2022), p. 147.

[18] F.J. Yao, D.J. Li, Z.X. Li, B. Hu, Y. Huang, and X.Q. Zeng, Ultra-high thermal conductivity of Mg–4Sm–2Al alloy by MWCNTs addition, *Mater. Lett.*, 341(2023), art. No. 134224.

[19] C.Y. Su, D.J. Li, A.A. Luo, T. Ying, and X.Q. Zeng, Effect of solute atoms and second phases on the thermal conductivity of Mg–RE alloys: A quantitative study, *J. Alloys Compd.*, 747(2018), p. 431.

[20] X.X. Dong, L.Y. Feng, S.H. Wang, *et al*., A quantitative strategy for achieving the high thermal conductivity of die-cast Mg–Al-based alloys, *Materialia*, 22(2022), art. No. 101426.

[21] Y.F. Liu, X.J. Jia, X.G. Qiao, S.W. Xu, and M.Y. Zheng, Effect of La content on microstructure, thermal conductivity and mechanical properties of Mg–4Al magnesium alloys, *J. Alloys Compd.*, 806(2019), p. 71.

[22] M.F. Qi, L.Y. Wei, Y.Z. Xu, *et al*., Effect of trace yttrium on the microstructure, mechanical property and corrosion behavior of homogenized Mg–2Zn–0.1Mn–0.3Ca–*x*Y biological magnesium alloy, *Int. J. Miner. Metall. Mater.*, 29(2022), No. 9, p. 1746.

[23] M. Rodchom, P. Wimuktiwan, K. Soongprasit, D. Atong, and S. Vichaphund, Preparation and characterization of ceramic materials with low thermal conductivity and high strength using high-calcium fly ash, *Int. J. Miner. Metall. Mater.*, 29(2022), No. 8, p. 1635.
[24] G.H. Wu, C.L. Wang, M. Sun, and W.J. Ding, Recent developments and applications on high-performance cast magnesium rare-earth alloys, *J. Magnes. Alloys*, 9(2020), No. 1, p. 1.
[25] X.Q. Zeng, J. Wang, T. Ying, W.J. Ding, Recent progress on thermal conductivity of magnesium and its alloys, *Acta Metall. Sin.*, 58(2022), No. 4, p. 400.
[26] X.F. Zhao, Z.X. Li, W.K. Zhou, D.J. Li, M. Qin, and X.Q. Zeng, Effect of Al content on microstructure, thermal conductivity, and mechanical properties of Mg–La–Al–Mn alloys, *J. Mater. Res.*, 36(2021), No. 15, p. 3145.
[27] S.M. Zhu, M.A. Gibson, J.F. Nie, M.A. Easton, and T.B. Abbott, Microstructural analysis of the creep resistance of die-cast Mg–4Al–2RE alloy, *Scripta Mater.*, 58(2008), No. 6, p. 477.
[28] J.M. Kim, S.J. Lee, Microstructure and Castability of Mg–Al–La alloys for high conductivity applications, *Int. J. Metalcast.*, 9(2015), No. 3, p. 15.
[29] C. Wong, K. Nogita, M.J. Styles, *et al*., Solidification path and microstructure evolution of Mg–3Al–14La alloy: Implications for the Mg-rich corner of the Mg–Al–La phase diagram, *J. Alloys Compd.*, 784(2019), No. 5, p. 527.
[30] W.K. Zhou, Z.X. Li, D.J. Li, *et al.*, Comparative study of corrosion behaviors of die cast LA42 and AZ91 alloys, *J. Magnes. Alloys*, (2022). DOI: 10.1016/j.jma.2022.10.022
[31] E.Y. Guo, S.S. Shuai, D. Kazantsev, *et al*., The influence of nanoparticles on dendritic grain growth in Mg alloys, *Acta Mater.*, 152(2018), p. 127.
[32] C. Wong, M.J. Styles, S.M. Zhu, *et al*., $(Al,Mg)_3La$: A new phase in the Mg–Al–La system, *Acta Cryst.*, 74(2018), p. 370.
[33] J.H. Zhang, D.P. Zhang, Z. Tian, *et al*., Microstructures, tensile properties and corrosion behavior of die-cast Mg–4Al-based alloys containing La and/or Ce, *Mater. Sci. Eng. A*, 489(2008), No. 1-2, p. 113.
[34] L.Y. Feng, X.X. Dong, M.X. Xia, *et al*., Development of high thermal conductivity, enhanced strength and cost-effective die-cast Mg alloy compared with AE44 alloy, *J. Mater. Res. Technol.*, 22(2023), p. 2955.
[35] S.M. Zhu, C. Wong, M.J. Styles, T.B. Abbott, J.F. Nie, and M.A. Easton, Revisiting the intermetallic phases in high-pressure die-cast Mg–4Al–4Ce and Mg–4Al–4La alloys, *Mater. Charact.*, 156(2019), art. No. 109839.
[36] X. Zhang, L. Li, Z. Wang, *et al*., Ultrafine-grained Al–La–Mg–Mn alloy with superior thermal stability and strength-ductility synergy, *Mater. Sci. Eng. A*, 873(2023), art. No. 145035.
[37] X.K. Zhang, L.J. Li, Z. Wang, H.L. Peng, J.X. Gao and Z.W. Peng, A novel high-strength Al–La–Mg–Mn alloy for selective laser melting, *J. Mater. Sci. Technol.*, 137(2023), No. 20, p. 205.
[38] C. Liu, Q. Luo, Q.F. Gu, Q. Li, and K.C. Chou, Thermodynamic assessment of Mg−Ni−Y system focusing on long-period stacking ordered phases in the Mg-rich corner, *J. Magnes. Alloys*, 10(2022), No. 11, p. 3250.
[39] H.C. Chen, W. Xu, Q. Luo, *et al*., Thermodynamic prediction of martensitic transformation temperature in Fe–C–*X* (*X* = Ni, Mn, Si, Cr) systems with dilatational coefficient model, *J. Mater. Sci. Technol.*, 112(2022), p. 291.
[40] Q. Zhang, H.C. Chen, Q. Luo, Y. Yuan, H.Q. Liu, and Q. Li, The design of Ti–Cu–Ni–Zr titanium alloy solder: Thermodynamic calculation and experimental validation, *J. Mater. Sci.*, 57(2022), No. 12, p. 6819.
[41] S. Zhang, Q.Q. Li, H.C. Chen, Q. Luo, and Q. Li, Icosahedral quasicrystal structure of the $Mg_{40}Zn_{55}Nd_5$ phase and its thermodynamic stability, *Int. J. Miner. Metall. Mater.*, 29(2022), No. 8, p. 1543.
[42] Q. Luo, C. Zhai, Q.F. Gu, W.F. Zhu, and Q. Li, Experimental study and thermodynamic evaluation of Mg–La–Zn system, *J. Alloys Compd.*, 814(2020), art. No. 152297.
[43] Q. Luo, C. Zhai, D.K. Sun, W. Chen, and Q. Li, Interpolation and extrapolation with the CALPHAD method, *J. Mater. Sci. Technol.*, 35(2019), No. 9, p. 2115.
[44] L. Huang, S.H. Liu, Y. Du, and C. Zhang, Thermal conductivity of the Mg–Al–Zn alloys: Experimental measurement and CALPHAD modeling, *Calphad*, 62(2018), p. 99.
[45] C. Zhai, Q. Luo, Q. Cai, R.G. Guan, and Q. Li, Thermodynamically analyzing the formation of $Mg_{12}Nd$ and $Mg_{41}Nd_5$ in Mg–Nd system under a static magnetic field, *J. Alloys Compd.*, 773(2019), p. 202.
[46] Y. Wang, H.J. Kang, Y. Guo, H.T. Chen, M.L. Hu, and Z.S. Ji, Design and preparation of aluminum alloy with high thermal conductivity based on CALPHAD and first-principles calculation, *China Foundry*, 19(2022), No. 3, p. 225.
[47] C. Zhang, Y. Du, S.H. Liu, Y.L. Liu, and B. Sundman, Thermal conductivity of Al–Cu–Mg–Si alloys: Experimental measurement and CALPHAD modeling, *Thermochim. Acta*, 635(2016), p. 8.
[48] M. Hosseinifar and D.V. Malakhov, On the fabricability of a composite material containing the FCC matrix with embedded ductile B2 intermetallics, *J. Alloys Compd.*, 505(2010), No. 2, p. 459.
[49] J.M. Joubert, B. Kaplan, and M. Selleby, The specific heat of Al-based compounds, evaluation of the Neumann–Kopp rule and proposal for a modified Neumann-Kopp rule, *Calphad*, 81(2023), art. No. 102562.
[50] D.K. Lee, J. In, and S. Lee, Standard deviation and standard error of the mean, *Korean J. Anesthesiol.*, 68(2015), No. 3, p. 220.
[51] C.Y. Su, D.J. Li, A.A. Luo, R.H. Shi, and X.Q. Zeng, Quantitative study of microstructure-dependent thermal conductivity in Mg–4Ce–*x*Al–0.5Mn alloys, *Metall. Mater. Trans. A*, 50(2019), No. 4, p. 1970.
[52] C.Y. Ho, M.W. Ackerman, K.Y. Wu, *et al*., Electrical resistivity of ten selected binary alloy systems, *J. Phys. Chem. Ref. Data*, 12(1983), No. 2, p. 183.
[53] H. Shi, Q. Li, J.Y. Zhang, Q. Luo, and K.C. Chou, Re-assessment of the Mg–Zn–Ce system focusing on the phase equilibria in Mg-rich corner, *Calphad*, 68(2020), art. No. 101742.